July 23-27, 2006, Vancoucer, BC, Canada

PVP2006-ICPVT-11-93562

ANALYSIS OF MULTIPLE CO-PLANAR SURFACE BREAKING FLAWS LOADED IN TENSION UNDER CLEAVAGE FAILURE CONDITIONS

J K Sharples, M A Wilkes, S F Yellowlees, D W Beardsmore, G T Melvin, R Hurlston
Serco Assurance, Birchwood Park, Warrington, Cheshire, WA3 6GA, UK

C T Watson
Rolls-Royce plc, Derby, PO Box 2000, DE21 7XX, UK

ABSTRACT

In procedures such as R6 and BS 7910 for assessing the structural integrity of structures, complex multiple flaws located in close proximity to each other are generally characterised as one, larger, single flaw. Recent studies have shown that the current characterisation rules may be non-conservative under some circumstances.

Concurrent experimental and analytical programmes are being undertaken in order to further investigate this potential non-conservatism for situations where the possibility of cleavage failure has to be taken into account when assessing structures or components containing multiple flaws.

The analytical work has involved inelastic finite element modelling in conjunction with numerical analysis based on the weakest link methodology for cleavage initiation to determine the probability of cleavage failure. This has allowed the probability of failure for the situation of multiple adjacent flaws to be compared with that for the single characterised flaw to determine whether the characterisation rules are conservative.

Initial results from the cases studied so far indicate that:

- For flaws that do not touch, the probability of cleavage failure for the single characterised flaw is higher than the original flaws, confirming that the characterisation process is conservative in this case (perhaps significantly so).
- For low aspect ratio (depth/length << 1.0) flaws in contact, the probability of cleavage failure for the single characterised is higher than the original flaws, confirming that the characterisation process is conservative in this case.
- However, for high aspect ratio (depth/length ~ 1.0) flaws in contact, the probability of cleavage failure for the single characterised flaw is lower than the original flaws, indicating that the characterisation process may be non-conservative in this case.

This paper covers the initial stages of a much larger programme. The analyses presented in this paper are in the process of being extended to allow for crack-tip constraint effects. Early results from these further analyses indicate that the loss of constraint between interacting flaws may be a significant factor and could eliminate at least some of the perceived non-conservatism for the high aspect ratio flaw. Further work is also underway to examine the effect of any localised coalescence of defects (a re-entrant region); the current analyses consider defects that are only just in contact. Further papers are therefore expected.

INTRODUCTION

In order to assess the effect of multiple interacting flaws using the methodologies such as R6 [1] or BS 7910 [2], it is necessary to characterise the flaws into a single, larger flaw that can then be assessed. Recent experimental studies of components with interacting surface-breaking flaws in bending [3,4] have shown that the characterisation rules may be non-conservative in the case of cleavage fracture.

To investigate this further, finite element (FE) analyses have been undertaken of a postulated test component with two surface-breaking semi-elliptical flaws. In this case the loading is assumed to be tensile. The flaws have been assumed to be identical, coplanar, and either in contact or closely-spaced. To assess the conservatism of the characterisation procedure, the characterised

flaws have also been modelled. In addition, a complementary experimental programme is underway to investigate this important issue. Details and results of the first phase of analytical work are presented below, together with a brief overview of the experimental work being undertaken.

FINITE ELEMENT ANALYSES

In the previous studies [3,4], it was postulated that the increase in cleavage failure probability for closely-spaced flaws was associated with elevated levels of crack driving force in the region where the defects are closest, and may be particularly prevalent if the defect coalesce locally (termed as a re-entrant feature in previous work). The studies presented in this paper primarily consider defects that are close, or indeed just touching. Some preliminary work has been carried out to consider these re-entrant features and further work is already underway. A schematic of the flaw geometries is shown in Figure 1.

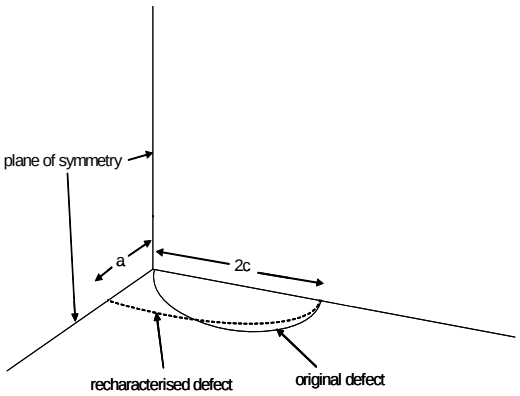

Figure 1: Schematic of Models

The failure probability has been estimated using a method based on integration of the stress intensity factor along the crack front. The levels of crack tip constraint have also been estimated, via the T-stress parameter.

The cases are numbered according to the following rule:

Case number =T/B<ijj>A/C<n>

where T = tensile loading, B = bending loading[1]
A = actual (original) flaw, C = characterised flaw
i = 1 for a/c=0.8, 2 for a/c=0.44
jj = separation *s* in mm

The cases studied to date are:

- T100A: Twin flaws of length 25mm and depth 10mm, in contact.
- T100C: Single flaw of length 50mm and depth 10mm (characterisation of T100A).
- T110A: Twin flaws of length 25mm and depth 10mm, separated by 10mm.
- T110C: Single flaw of length 60mm and depth 10mm (characterisation of T110A).
- T200A: Twin flaws of length 45mm and depth 10mm, in contact.
- T200C: Single flaw of length 90mm and depth 10mm (characterisation of T200A).

[1] This paper only covers the tension case but is part of a wider programme with further papers being published.

Modelled Specimen

The model represents a plate of dimensions 150x25mm with either single or twin surface-breaking semi-elliptical flaws. Use has been made of planes of symmetry to reduce model size; one symmetry plane is in the crack plane, the other is orthogonal to this, passing halfway between the flaws, or through the flaw minor axis in the characterised flaw (Figure 1). The specimen has been modelled to a length of 100mm. The dimensions were chosen so as to be consistent with the previous experimental studies [3,4].

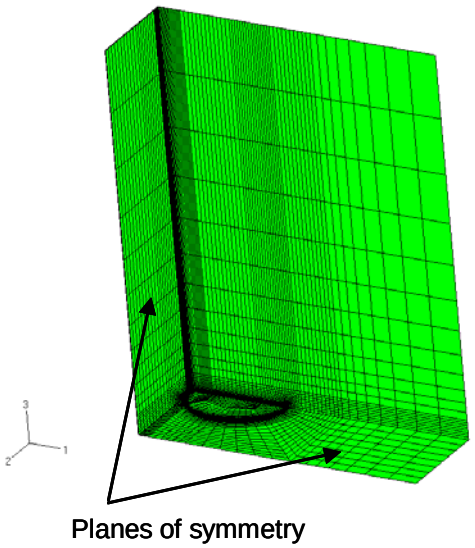

Figure 2: Case T100A Mesh Overview

Meshing

In all cases, the FE meshes were generated using the IDEAS pre-processing package [5], combined with direct ABAQUS [6] command input. The models consist of 3D linear elements for stress-displacement analysis (type C3D8). An example of the mesh is given in Figure 2.

Material Properties

For consistency, material properties relevant to the recently reported work [3,4] have been used in the analyses. The yield stress (σ_0) is 640 MPa, with a work-hardening coefficient (n) of 9. The stress-strain curve has been generated using the relation:

$$\frac{\varepsilon}{\varepsilon_0} = \frac{\sigma}{\sigma_0}, \qquad \text{for } \sigma < \sigma_0 \qquad (1)$$

$$\frac{\varepsilon}{\varepsilon_0} = \frac{\sigma}{\sigma_0} + \alpha\left(\frac{\sigma - \sigma_0}{\sigma_0}\right)^n, \ \text{for } \sigma > \sigma_0 \qquad (2)$$

Stress-plastic strain data were supplied to ABAQUS as tabulated data pairs for strains up to 1. The elastic modulus, E,

is 221GPa, while Poissons ratio, υ, is 0.3. These properties are appropriate to 50D steel for a temperature of -196°C.

Loads and Boundary Conditions

As described above, the model has symmetry in the crack plane and orthogonal to the crack plane at the flaw centreline (Figure 1). In addition, the node at the corner of the plate was constrained in the y (through-thickness) direction to avoid the occurrence of rigid-body modes. The model was loaded in tension via a concentrated load applied at the top face, acting over all of the top face nodes via an EQUATION condition that enforces planar movement.

In all cases, the maximum load applied corresponded to a value of 50% of the plastic limit load. The limit load was determined by means of an analysis using elastic-perfectly plastic material properties. The definition of limit load used here is the local limit load, i.e. where plasticity breaks through from the flaw to the opposite face of the model. The value of this limit load is dependent on the flaw size; it was found, in terms of applied stress, to be 500MPa for the a=10mm, 2c=45mm cases (Cases T2xx) and 541MPa for the a=10mm, 2c=25mm cases (Cases T1xx). The stress applied to achieve 50% limit load (i.e. $L_r = 0.5$ in terms of the R6 failure assessment diagram) was therefore 250MPa for Cases T2xx and 270.5MPa for T1xx. The same load was used for the characterised flaws in order to get a like-for-like comparison of the probability of cleavage. It should be noted that the results for the characterised defects are quoted in terms the L_r values for the original defect. Results were extracted at intervals of $L_r = 0.025$.

Results

The probability of cleavage from an evaluation of K_J around the crack front

For each analysis, values of *J*-integral and *T*-stress were output along the flaw front. The J values were converted to K_J via the relation

$$K_J = \sqrt{\frac{EJ}{\left(1-\nu^2\right)}} \qquad (3)$$

In the cases where the flaws were in contact, it was not possible to obtain a value of J for the point at the apex where the flaws touch; K_J for this point was derived by extrapolation from adjacent points.

By weakest link statistics, the failure probability for the flaw can be obtained by considering the product of survivor functions of infinitesimal lengths all along the flaw front. Each survivor function is given by the exponential term in the Master Curve equation [7, 8]. Integrating and scaling for length gives:

$$P_F = 1-\exp\left\{-\frac{1}{B_0}\int_0^L\left(\frac{K_J(l)-K_{\min}}{K_0-K_{\min}}\right)^4 dl\right\} \qquad (4)$$

This form is consistent with the Master Curve equation for a straight-fronted flaw and constant K_J (e.g. plane strain fracture toughness specimens).

Recasting Eq. (4) into a form more appropriate to the FE model results in:

$$P_F = 1-\exp\left\{-\frac{2}{B_0}\sum_{i=1}^{n}\left(\frac{K_J(i)-K_{\min}}{K_0-K_{\min}}\right)^4 \Delta l_i\right\} \qquad (5)$$

where $K_J(i)$ is the value of K_J for a one-element 'slice' number *i* of the crack front, evaluated as the mean of the nodal values at each end of the slice and Δl_i is the slice length. The factor K_{min} is taken as 20MPa√m and B_0 as 25mm. K_0 is given by [8]:

$$K_0 = 31+77*\exp(0.019*(T-T_0))$$

where *T* is the temperature (-196°C) and T_0 is -130°C [3,4].

The factor of 2 in Eq. (5) is introduced to account for symmetry.

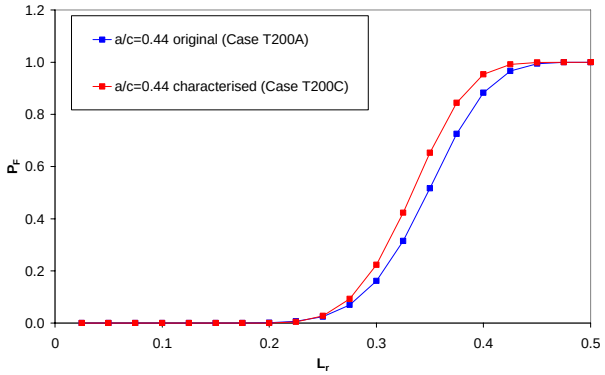

Figure 3: P_F vs. L_r for Cases T200A/C

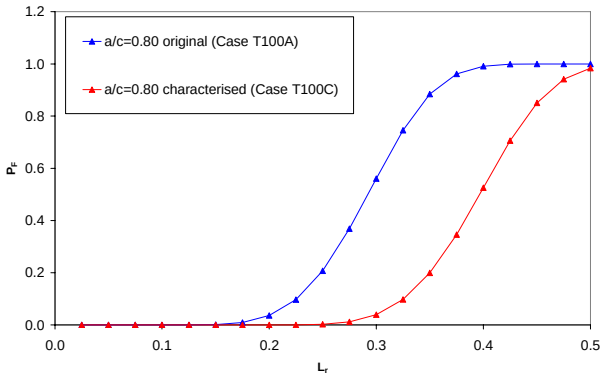

Figure 4: P_F vs. L_r for Cases T100A/C

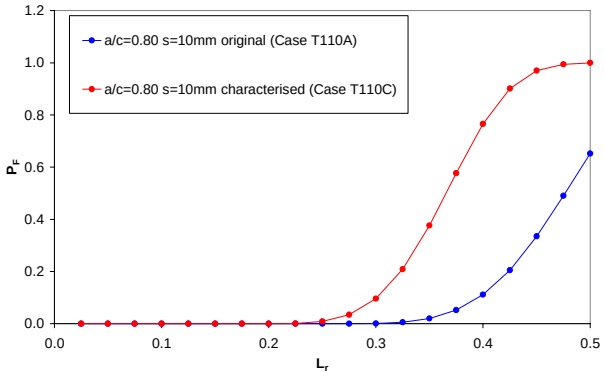

Figure 5: P_F vs. L_r for Cases T110A/C

Plots of P_F against L_r are shown in Figures 3 (Cases T200A/C), 4 (cases T100A/C) and 5 (Cases T110A/C). It can be seen that for the characterisation of Case T200 (Figure 3), P_F is slightly over-predicted using the characterised defect, demonstrating that the characterisation process is slightly conservative in this case.

However, for Case T100A, the characterisation (T100C) leads to a large non-conservatism in P_F (Figure 4). The characterisation of Case T110A by Case T110C produces an increase in P_F (Figure 5), demonstrating a significant level of conservatism in the case where the flaws are separated. There is thus some significant variability in the level of conservatism (or otherwise) and further investigation of the results was carried out.

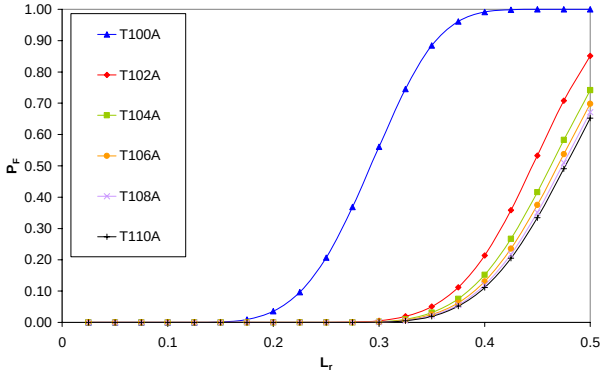

Figure 6: P_F vs. L_r for Cases T100A-T110A

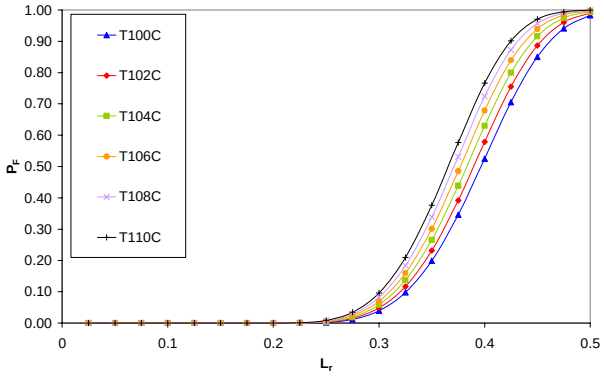

Figure 7: P_F vs. L_r for Cases T100C-T110C

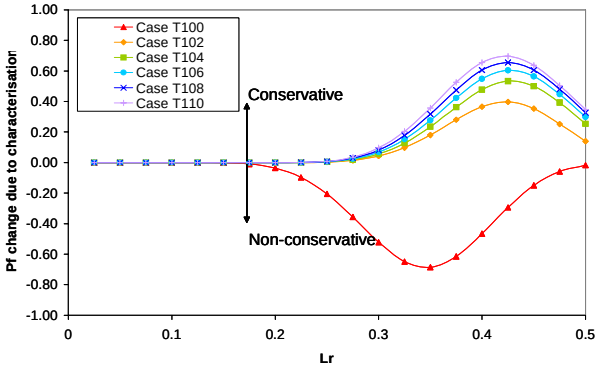

Figure 8: Difference in P_F vs. L_r for Cases T100-T110

To understand the influence of flaw separation on P_F, the analyses were repeated for intermediate separations in increments of 2mm (Cases T102-108). The results for the original defects are shown in Figure 6. It can be seen that P_F increases gradually as the separation is reduced from 10mm to 2mm, but there is then a large increase in P_F from 2mm to zero. This can be contrasted with the behaviour of the characterised defects (Figure 7) where there is a modest and gradual increase in P_F for the cases representing defects with separations from zero to 10mm. Plotting the differences in P_F between the original and characterised defects (Figure 8) demonstrates that the non-conservatism occurs only when the defect separation is very small.

To examine these results further, the values of K_J have been plotted for the case of L_r=0.5 for all of the flaws. Since the calculation of P_F depends on K_J, this should reveal which parts of the flaw are contributing to the failure probability. For consistency, the plots are made against the distance along the flaw major axis, with zero at the plane of symmetry. Thus, for the 10mm separated flaws (case T110A), the plot begins at 5mm.

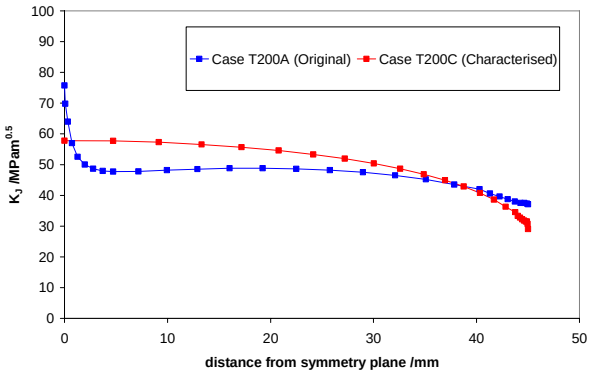

Figure 9: K_J for Cases T200A/C

Figure 9 shows K_J for Cases T200A and T200C. This plot clearly shows that while the characterised flaw (Case T200C) gives rise to higher K_J along most of the flaw length, there is a localised region of high K_J for the original (Case T200A) flaw where the defects touch. K_J is also higher for Case T200A at the far end of the flaw. Since the contribution to failure probability is proportional to the 4th power of K_J (Eqs. (4) and (5)), this region produces a sufficiently large contribution to cause the probability

to be higher than that for case T200C. There is also a contribution due to the greater length of the crack front for Case T200A.

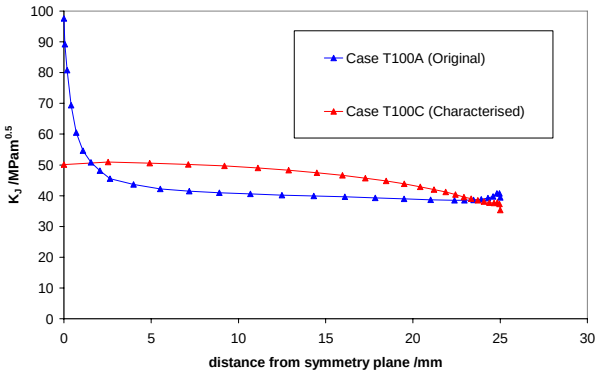

Figure 10: K_J for Cases T100A/C

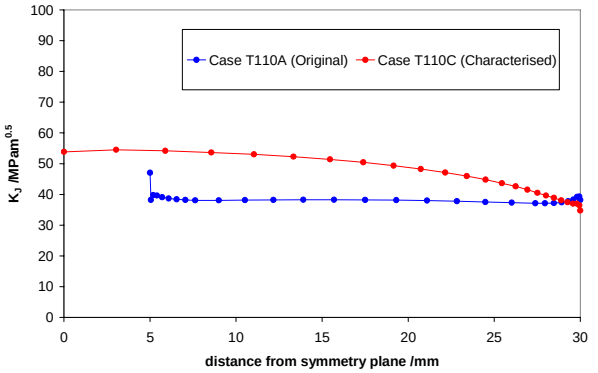

Figure 11: K_J for Cases T110A/C

For the 25mm flaw (Case T100A) a similar effect is seen (Figure 10). However, in this case the enhancement of K_J in the re-entrant region of the representations of the original flaw (Case T100A) is larger than that seen for case T200, giving rise to a correspondingly larger increase in cleavage probability.

For Case T110A (the separated 25mm flaw) and its characterised flaw (Case T110C), the opposite applies. Case T110A (Figure 11) exhibits only a slight enhancement of K_J where the defects are closest. This enhancement is comparable with that seen at the corresponding intersection of the distal end (with only a small very localised additional peak), suggesting that the flaws are sufficiently far apart for interaction to be small. K_J for Case T110A is therefore lower than that for Case T110C over the entire flaw with the exception of a small region around the distal intersection; this gives rise to a lower calculated failure probability than that due to the re-characterised flaw.

The effect of constraint

However, in the regions where the K_J is highest, there is also the potential for loss of constraint. This may offset the significance of these local increases in K_J. Elastic analyses were performed (at a load corresponding to L_r=0.5) to obtain T-stress values around the crack tip. These are plotted in Figures 12 (Case T200A/C), 13 (Case T100A/C) and 14 (Case T110A/C).

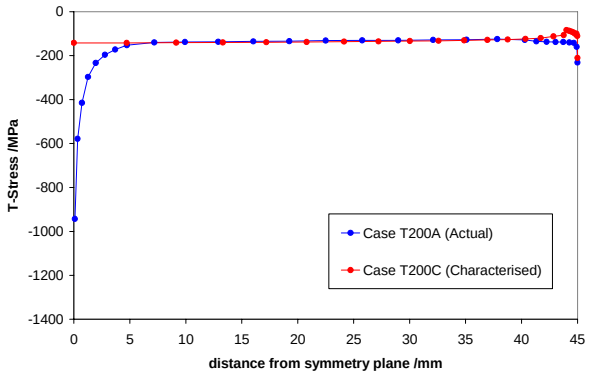

Figure 12: T-Stress for Cases T200A/C

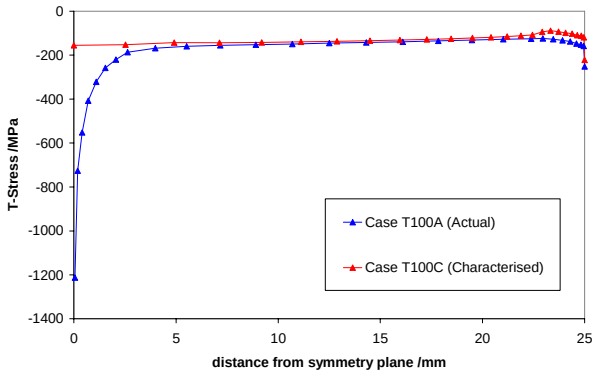

Figure 13: T-Stress for Cases T100A/C

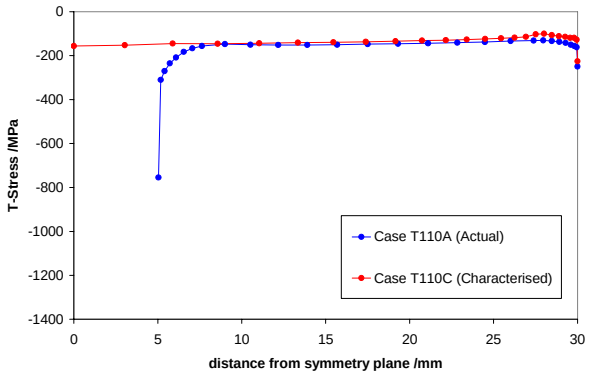

Figure 14: T-Stress for Cases T110A/C

It should be noted that the values of K_J shown in Figures 9, 10 and 11 and the values of T-stress shown in Figures 12, 13 and 14 for the surface points of the twin flaws have been extrapolated (from the near-surface values) rather than taken from the actual surface nodes. This is because there are significant numerical inaccuracies in calculating these parameters at the surface.

It can be seen that for all of the original (twin flaw) models, constraint remains fairly constant around the majority of the crack front. A limited amount of constraint loss is associated with the distal end of the flaw. However, there is a large loss of constraint where the defects are closest for Cases T200A, T100A and T110A.

The characterised flaws also exhibit a small constraint loss at the outer end, but the *T*-stress remains fairly constant elsewhere.

The failure probability evaluations presented above are therefore in the process of being extended to incorporate crack-tip constraint effects based on the *T*-stress values, since this could reduce or eliminate the non-conservatism implied by the analyses above.

EXPERIMENTAL PROGRAMME

The experimental programme on co-planar flaws is consistent with part of the finite element analysis work referred to above in that the first stage is addressing the T100A (twin semi-elliptical surface flaws of length 25mm and depth 10mm in contact) and T100C (single flaw of length 50mm and depth 10mm; characterisation of T100A) cases. In order to try and allow for scatter effects in the results, three fracture experiments are being carried out for each of these cases. The flaws are initially manufactured into the plate by the spark erosion process and then sharpened by fatigue crack growth under four-point-bending to approximately the required dimensions. The plate dimensions are 100x25mm (again consistent with the FE modelling) and the material is EN100255 355 J2G3, which is equivalent to 50D, the material used in the previous studies [3,4]. The tensile fracture experiments are being carried out in a 2.5 MN testing machine. The flaw size during the fatigue pre-cracking is being monitored by a combination of ACPD monitoring (for growth in the depth direction) and an optical method (for growth at the surface). During the fracture experiments, strain gauges placed on both surfaces are monitored in order to check that no out-of-plane bending is occurring. The experiments are conducted under displacement controlled loading at a temperature of -196^{o}C using liquid nitrogen. Plots of applied load vs actuator displacement are shown for the three T100A experiments in Figure 15. The failure (cleavage) loads for these three experiments were 680, 765 and 656 kN. From the three characterised flaw specimens that have been tested, the failure (cleavage) loads were 741kN, 605kn and 770kN. It is now necessary to measure the actual defect sizes in the specimens after pre-cracking and carry out specific analyses to interpret these results. Future papers will bring together all analytical and experimental results.

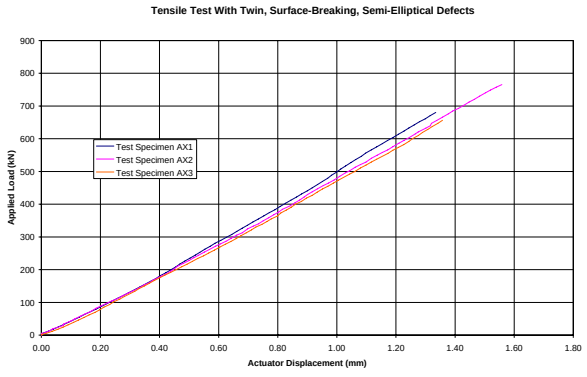

Figure 15: Load vs Actuator Displacement

Other co-planar flaw experiments (cleavage) to be carried out will be on specimens containing elliptically embedded flaws again loaded under tension. A series of non-coplanar flaw experiments (cleavage) will also be undertaken on specimens containing semi-elliptical surface flaws under bending.

CONCLUSIONS

Finite element representations of coplanar surface-breaking semi-elliptical twin flaws, and the corresponding characterised flaws, have been developed. Using these models, finite element analyses have been performed to evaluate cleavage failure probabilities due to tensile loading in the low L_r regime.

For flaws that do not touch, the probability of cleavage failure for the single characterised flaw is higher than the original flaws, confirming that the characterisation process is conservative in this case (perhaps significantly so).

For low aspect ratio (depth/length << 1.0) flaws in contact, the probability of cleavage failure for the single characterised is higher than the original flaws, confirming that the characterisation process is conservative in this case.

However, for high aspect ratio (depth/length ~ 1.0) flaws in contact, the probability of cleavage failure for the single characterised flaw is lower than the original flaws, indicating that the characterisation process may be non-conservative in this case.

Values of *T*-stress from elastic analyses reveal a localised loss of constraint where the two defects are closest. This loss of constraint may be beneficial. The failure probability evaluations presented in this paper are therefore in the process of being extended to incorporate crack-tip constraint effects based on the *T*-stress values. Early results from these further analyses indicate that the loss of constraint between interacting flaws may be a significant factor and could eliminate at least some of the perceived non-conservatism for the high aspect ratio flaw.

It is also important to examine the effect of any localised coalescence of defects (a re-entrant region). A limited number of analyses have been undertaken with such features. These suggest that the influence of the re-entrant is complex and results will be presented in a future paper after further analyses have been completed.

A brief overview of the experimental programme being undertaken has been given together with some preliminary results. All analytical and experimental results will be brought together in future published papers when further specific analyses of the experiments have been completed.

REFERENCES

1. "R6: Assessment of the Integrity of Structures Containing Flaws", British Energy Generation Limited, Revision 4 (2001).
2.. BS 7910:2005, "Guide to Methods for Assessing the Acceptability of Flaws in Metallic Structures", British Standards Institution.
3.. B Bezensek and J W Hancock, "The Re-characterisation of Complex Flaws. Part 1: Fatigue and Ductile Tearing", Eng. Fract. Mech., 71 (2004) p981-1000.
4. B Bezensek and J W Hancock, "The Re-characterisation of Complex Flaws. Part 2: Cleavage", Eng. Fract. Mech., 71 (2004) p1001-1019.
5. "I-DEAS Master Series 8", SDRC Inc.
6. "ABAQUS Version 6.4-1", ABAQUS Inc., 2004.
7. "Technical Basis for an ASTM Standard on Determining the Reference Temperature, T_0, FOR Ferritic Steels in the Transition Range", Prepared by J G Merkle, K Wallin, D E McCabe for US Nuclear Regulatory Commission,

NUREG/CR-5504, ORNL/TM-13631, 1998.
8. “ASTM Standards, E1921-98, Standard Test Method for Determination of Reference Temperature, T_0, for Ferritic Steels in the Transition Range, Section 3, Vol. 03.01, 1068-1084 (1998).

ACKNOWLEDGEMENTS
This paper is published by permission of Rolls Royce plc. and Serco Assurance.